Journal of Russian Laser Research, Volume 29, Number 2, 2008

CHARACTERIZATION OF POLYCRYSTALLINE Ge THIN FILMS FABRICATED BY SHORT-PULSE XeF EXCIMER LASER CRYSTALLIZATION

Chil-Chyuan Kuo

Department of Mechanical Engineering and Graduate Institute of Electro-Mechanical Engineering
Mingchi University of Technology
Gungjuan Road, 84, Taishan, Taipei, Hsien 243, Taiwan, R.O.C.
e-mail: jacksonk@mail.mit.edu.tw

Abstract

XeF excimer laser-induced melting and recrystallization dynamics of amorphous germanium are investigated using time-resolved optical reflection and transmission measurements with a nanosecond time resolution, field-emission scanning electron microscopy, and micro-Raman spectroscopy. It is found that the disc-shaped grain with a diameter of approximately 0.8 μm is located in the complete melting regime with a melt phase duration of approximately 141–200 ns. The significant change of transmissivity is a key phenomenon revealing the excessive excimer laser fluence during excimer laser crystallization by in-situ optical measurements. Differences between the melting and recrystallization phenomenon for Si and Ge thin films are also discussed.

Keywords: melting and recrystallization dynamics, amorphous germanium, excimer-laser crystallization, polycrystalline germanium.

1. Introduction

Liquid crystal displays are gaining importance as man–machine interfaces in devices, such as mobile phones and personal digital assistants, in our highly sophisticated information society. Consequently, high-performance thin-film transistors (TFTs) are essential for obtaining high-quality display devices with low power consumption. Excimer-laser crystallization (ELC) of amorphous semiconductors is a promising technique for the fabrication of large-area polycrystalline films in flat panel displays.

Fabrication of polycrystalline-Ge (poly-Ge) thin films by ELC is attractive for its application to high-performance TFTs because crystalline Ge has a hole mobility four times higher than that of silicon [1] and can realize high-speed electrical circuits on glass substrates [2] or flexible glass substrates [3]. In addition, poly-Ge thin films have shown a great potential to be a leading candidate as near-infrared detectors and tandem solar cells [4]. Until now, most investigations on laser crystallization of a-Ge have been carried out using continuous wave (CW) [5] or long-pulse laser [6]. Very few works have been reported, however, on the use of short-pulse excimer laser to fabricate poly-Ge thin films.

In this study, a short-pulse (25 ns) XeF excimer laser is employed for fabricating poly-Ge thin films. An in-situ time-resolved optical reflection and transmission (TRORT) [7–10] monitoring system combining a CW He–Ne probe laser, a digital oscilloscope, and two photodetectors is developed to investigate the

Manuscript submitted by the authors in English on December 18, 2007.

1071-2836/08/2902-0167 ©2008 Springer Science+Business Media, Inc.

melting and resolidification dynamics of a-Ge thin films during ELC. The melt-mediated transformation scenarios of the Ge thin films are determined in terms of various excimer-laser fluences. After ELC, ex-situ microstructural analysis of the resulting poly-Ge thin films is investigated by field-emission scanning electron microscopy (FE-SEM) and micro-Raman spectroscopy. The difference between the melting and recrystallization phenomena for Si and Ge thin films is also discussed.

2. Experiment

Figure 1 shows the schematic illustration of the sample structure and experimental setup for measuring the melt duration of molten Ge during ELC. The sample had a stacked structure consisting of a 300-nm-thick buffer SiO_2 layer and a 90-nm-thick a-Ge layer formed on a 0.7-mm-thick non-alkali glass substrate (Corning 1737).

The a-Ge thin films are grown at 200°C in a dc magnetron sputtering system using high-purity (99.999 %) Ge targets under a residual pressure of the system of $2.2{\cdot}10^{-6}$ Torr and an operating Ar pressure of $5{\cdot}10^{-3}$ Torr with a deposition rate of 3.296 nm/s. Raman scattering measurements revealed that the as-deposited Si thin films have an amorphous structure with no appreciable traces of impurities. The a-Ge thin films are irradiated by a XeF excimer laser operating at a wavelength of 351 nm with a short pulse of 25 ns in full width at half maximum (FWHM) in air and at room temperatures. The specimen is moved to a new position following each ELC using developed man-machined interface. A slit ($2{\times}15$ mm^2) is employed to transform the incident Gaussian beam into a rectangular beam spot. During ELC, in-situ TRORT measurements are performed using a CW He–Ne probe laser operating at a wavelength of 632.8 nm for investigating the kinetics of the crystallization process. An aperture with a diameter of 0.3 mm is mounted in front of the He–Ne probe laser to increase the resolution of TRORT measurements. The He–Ne laser had a 37° of incidence from the normal of the sample's surface and focused on the center of the laser-irradiated spot. The reflected beam from the specimen is focused on the photodetector. The interference filter is mounted in front of the photodetector, allowing only red light from the He–Ne probe laser to contribute to the detected signal. The photodetectors are positioned optimally to get the maximum signal before optical measurements. A quartz beam splitter is employed to reflect 10% of the excimer laser beam to a photodetector for triggering a fast digital storage oscilloscope (sample rate of 2 GHz/s) which recorded the optical spectra. The response time of the entire TRORT monitoring system is approximately 1 ns.

After ELC, ex-situ microstructural analysis of the resulting poly-Ge thin films is performed using FE-SEM operated at an acceleration voltage of 15 kV (resolution of 1.5 nm) and micro-Raman spectroscopy. The grain size of poly-Ge thin films is estimated using FE-SEM after Secco etching to reveal the grain boundary [11]. The Raman spectra are obtained at RT using a Raman microscopy system in back-scattering mode. The system is equipped with an optical microscope for focusing the 514.5 nm excitation source from the Ar^+ ion laser beam with a spot size of 5 μm (resolution of 2 cm^{-1}) onto the sample for the purpose of evaluating crystallinity fluctuation.

3. Results and Discussion

Figure 2 shows the transient excimer laser profile obtained by capturing scattered excimer laser light on a fast silicon photodetector with high resolution (response time ℓ = 300 ps). Figure 3 shows the

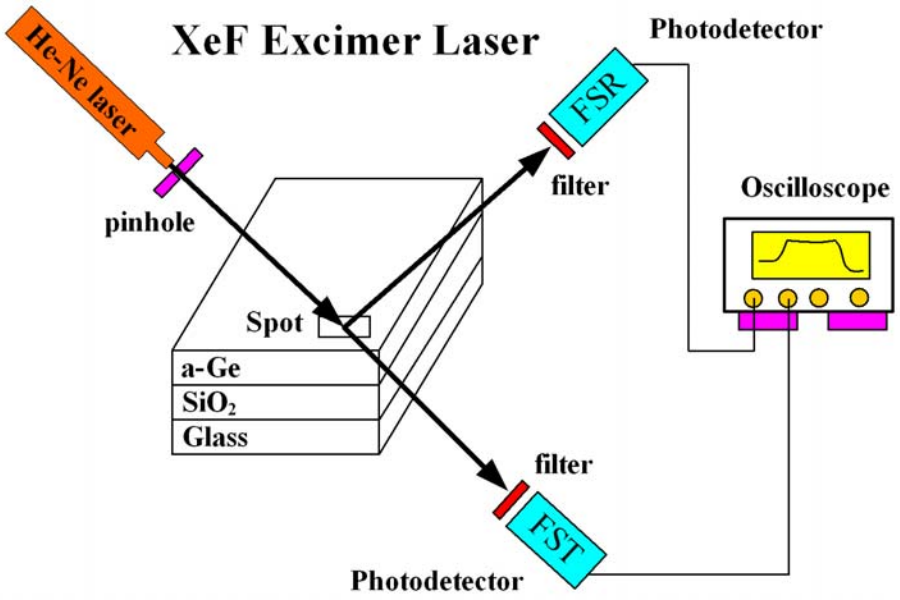

Fig. 1. Schematic illustration of the sample structure and experimental setup measuring the melt duration of molten Ge during ELC; FSR and FST represent the photodetector for receiving the frontside reflectivity and transmissivity during ELC, respectively.

correlation between the triggering signal, reflection signal, and transmission signal in this study. The response time of the reflection and transmission signals is delayed approximately 22 ns of the triggering signal. This delay is related to the time of a-Ge thin films for excimer laser absorption. The increase in the sample surface temperature caused by the probe laser has been determined by Solis and Afonso [12]. It is negligible for a-Ge thin films when compared with the excimer-laser-energy density during ELC because the increase in maximum surface temperature of the sample does not exceed 10 K. The SiO_2 layer does not directly absorb significant energy density from the XeF excimer laser, so it absorbs thermal energy by conduction from the Si layer underneath.

Below the surface melting threshold irradiation ($E < 70$ mJ/cm^2), the TRORT spectra exhibited an abrupt drop, followed by a relaxation to the initial value indicating that the a-Ge thin films did not melt but merely undergo heating and cooling during ELC. The changes in the TRORT spectra are governed by the temperature-dependent optical constants of Ge. Therefore, no poly-Ge in the sample can be observed using FE-SEM following ELC irradiation. This result is in good agreement with the observation of Si thin films by Boneberg and Leiderer [13].

Figure 4 shows time-resolved optical reflectivity spectra recorded by a fast digital storage oscilloscope during ELC of a-Ge thin films at various excimer laser fluences of 70–250 mJ/cm^2. When the a-Ge thin films are irradiated by excimer laser exceeding the surface melting threshold (70 mJ/cm^2), poly-Ge thin films can be observed by FE-SEM. This is also confirmed by the corresponding micro-Raman scattering spectra, as shown in Fig. 5. The sharp and symmetric peaks indicate that the microstructure of the a-Ge films has changed to poly-Ge films because the sharp peak of micro-Raman scattering spectra is centered at 297 cm^{-1}. Note that the FWHM of this spectra shows a value of 6–8 cm^{-1} when compared with bulk crystalline-Ge (1 cm^{-1}) [14]. Such difference can be attributed to the grain-size effects or to

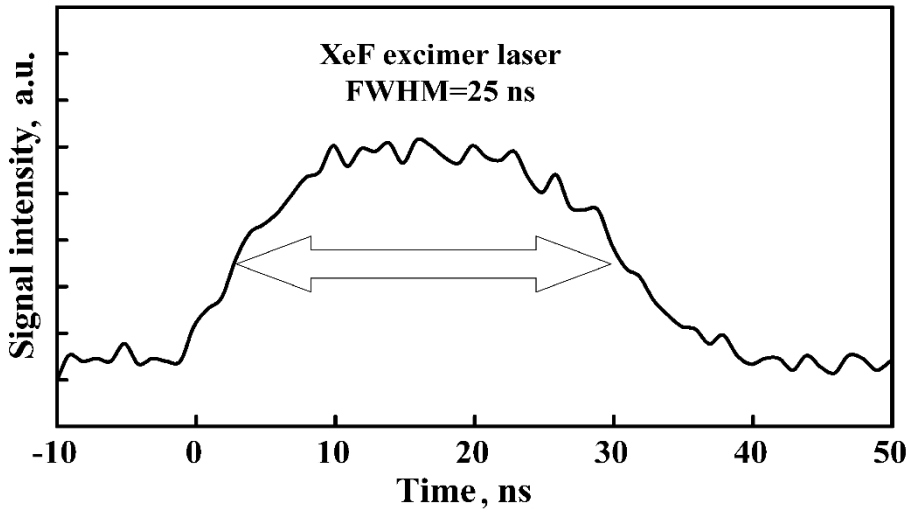

Fig. 2. Transient profile of XeF excimer laser pulse measured by a fast silicon photodetector. The FWHM of excimer laser pulse is 25 ns.

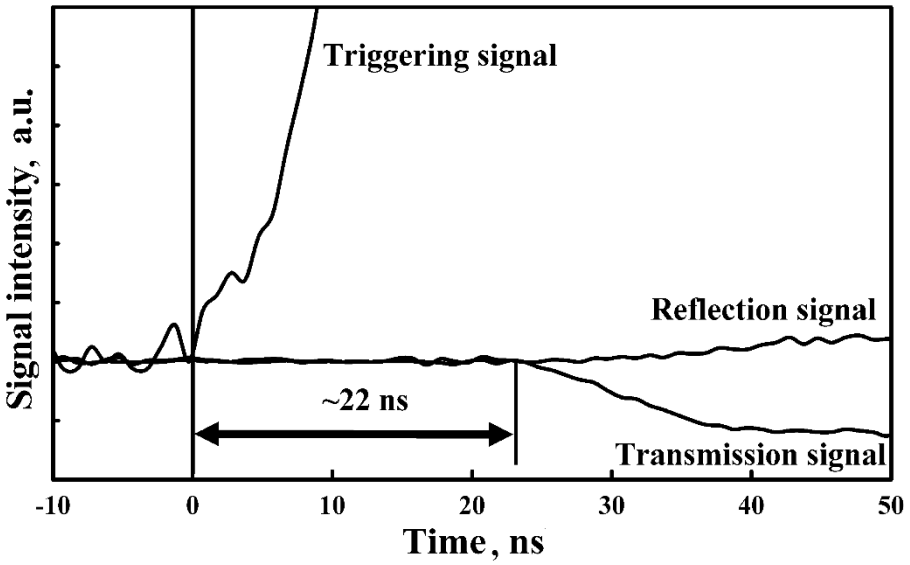

Fig. 3. Reflection and transmission signals versus triggering signal.

the existing internal strain [15], which plays an important role in excimer-laser crystallized amorphous semiconducting materials. Irreversible explosive amorphous to crystalline phase transformation has been reported by Messier et al. [16]. The heat released from the amorphous to crystalline phase transformation is additive to the heat loss from the irradiated region by conduction through the film, allowing further crystallization and grain growth along radial heat-flow directions. The velocity of the crystallization front in a-Ge thin films on glass substrate has been reported to be approximately 200 cm/s [5].

Figure 6 shows the TRORT spectra at excimer laser fluences of 200 mJ/cm^2. During excimer laser irradiation, the reflectivity increases due to the formation of molten Ge thin films with metallic-like reflectivity on the sample surface [17]. After excimer laser irradiation, the poly-Ge thin films are formed

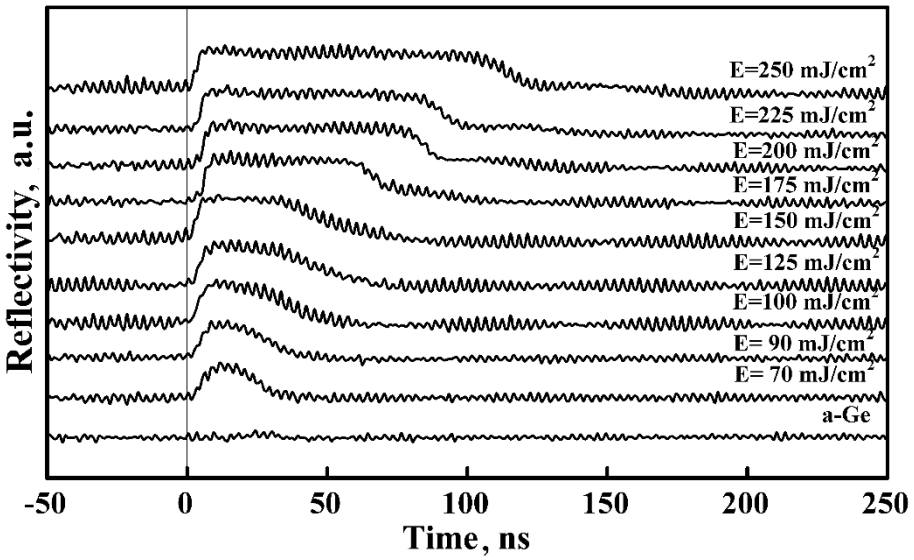

Fig. 4. Time-resolved optical reflectivity spectra recorded by a fast digital storage oscilloscope during ELC of a-Ge at various excimer laser fluences of 70–250 mJ/cm^2.

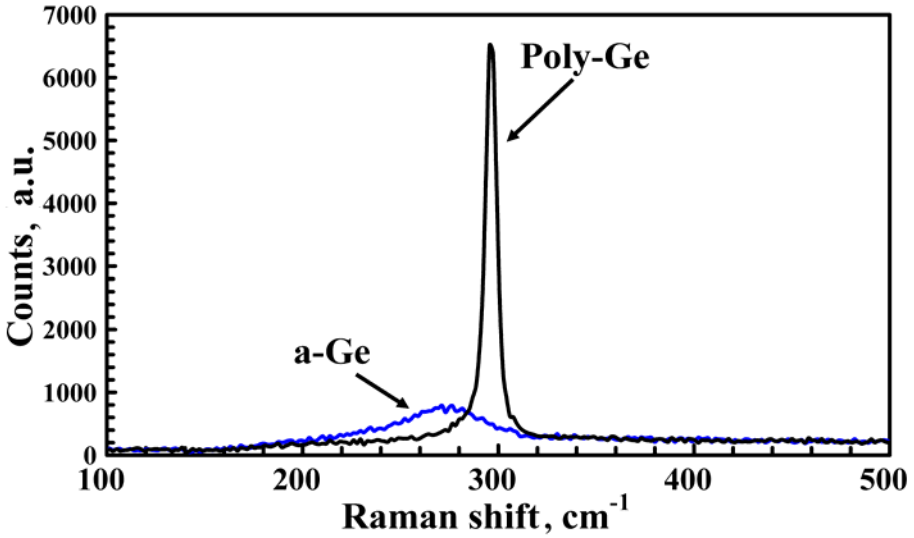

Fig. 5. Micro-Raman scattering spectra of a-Ge and poly-Ge.

due to the temperature decrease, and the interface moves toward the surface through heat diffusion into the substrate, causing a decrease in reflectivity. On the other hand, no significant change in the transmission signal is observed before and after excimer laser irradiation because the a-Ge and poly-Ge thin films are not transparent for the He–Ne probe laser.

Figure 7 shows the TRORT spectra at excimer laser fluences of 275 mJ/cm^2. FE-SEM results reveal that Ge thin films are ablated, causing some Ge thin films to be evaporated after excessive excimer laser irradiation. A striking phenomenon observed in this diagram is that the signal intensity of transmission exceeds the initial level of a-Ge, partial melting, and complete melting of Ge thin film. Correspondingly,

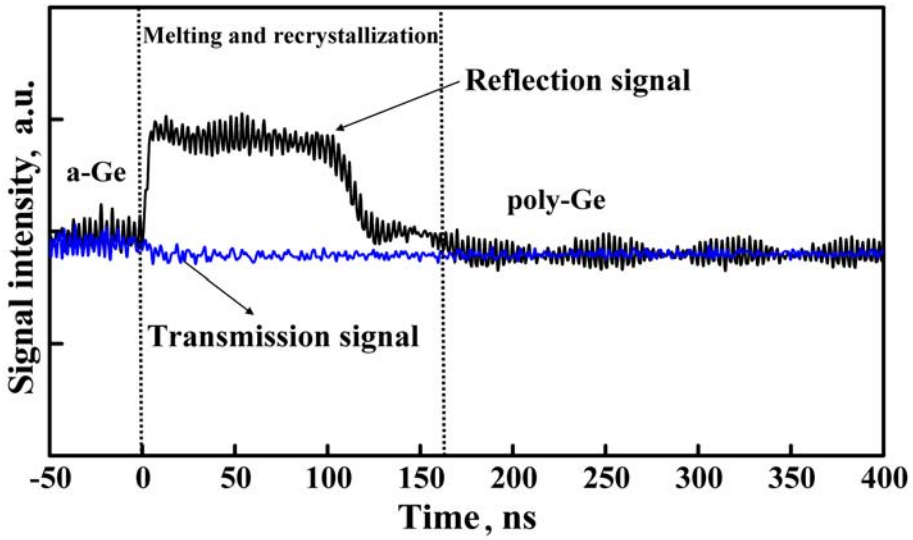

Fig. 6. TRORT spectra recorded by a fast digital storage oscilloscope during ELC of a-Ge at excimer laser fluences of 200 mJ/cm^2.

this phenomenon provides a rapid evaluation of excimer-laser fluence during mass production of high-performance TFTs using in-situ TRORT measurements. The main contribution of this observation can overcome the pulse-to-pulse fluctuation of excimer-laser fluence without using an expensive homogenizer during ELC [18].

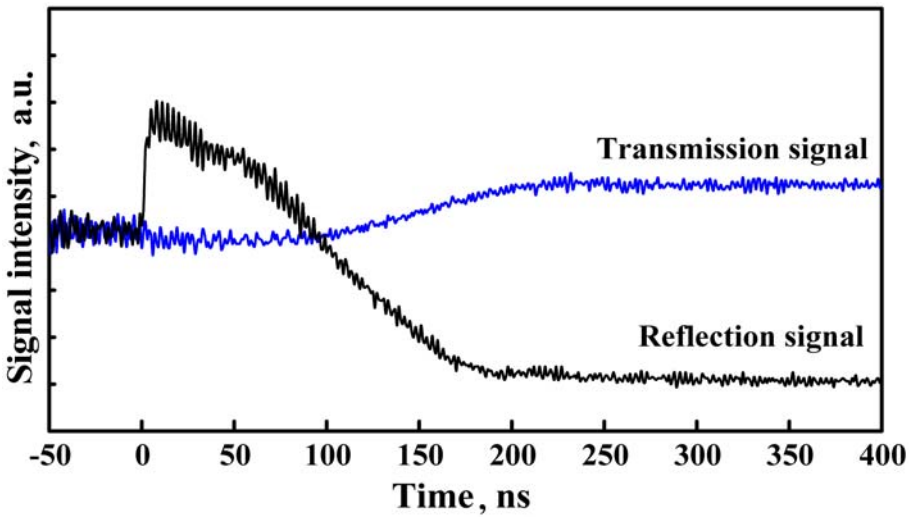

Fig. 7. TRORT spectra recorded by a fast digital storage oscilloscope during ELC of a-Ge at excimer-laser fluences of 275 mJ/cm^2.

Figure 8 shows the histogram of ablation excimer-laser fluence of a-Ge (sputter), a-Si (sputter), and a-Si (PECVD), respectively. It is apparent that the ablation excimer-laser fluence of a-Ge thin films is smaller than that of a-Si thin films fabricated by sputter or PECVD. These effects are mainly caused by the difference in melting temperature and thermal conductivity between Ge and Si thin films [19].

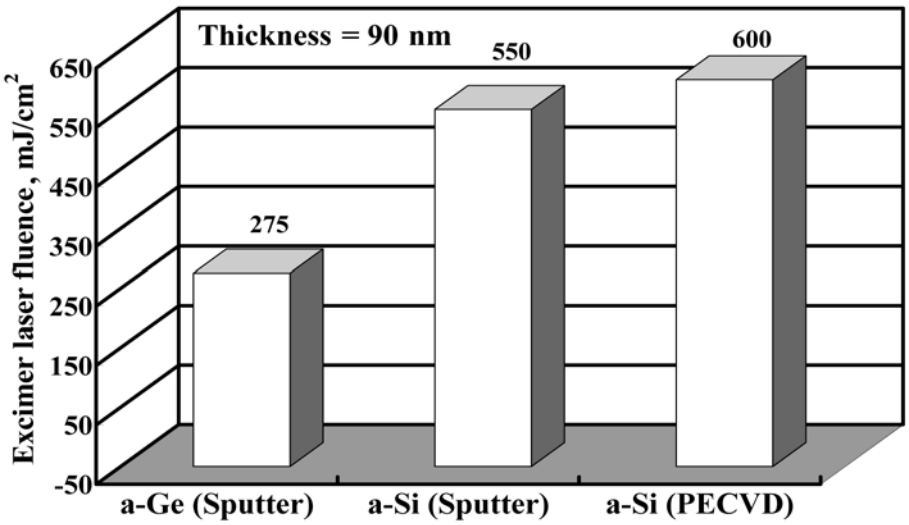

Fig. 8. Histogram of ablation excimer-laser fluence of a-Ge (sputter), a-Si (sputter), and a-Si (PECVD).

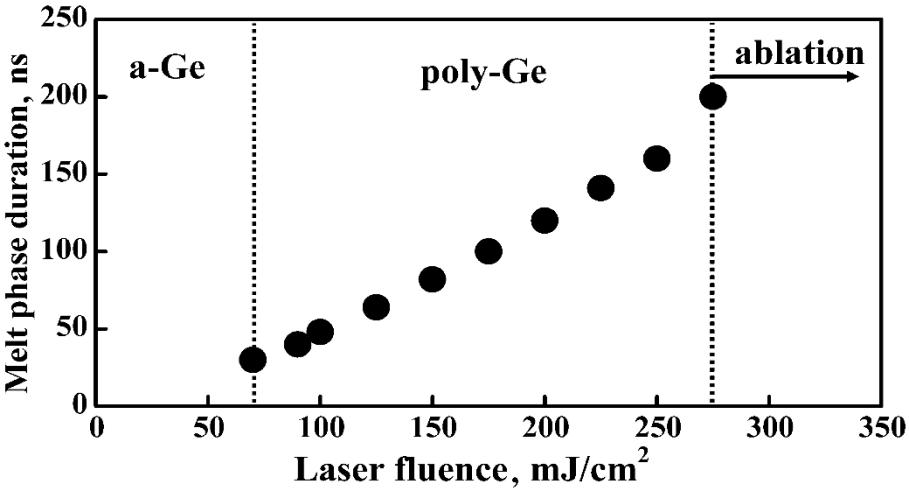

Fig. 9. Melt-phase duration as a function of excimer-laser fluence.

Figure 9 shows the melt-phase duration as a function of excimer laser fluence. The melt-phase duration increases with increasing excimer laser fluence from 70 to 250 mJ/cm^2. This means that the Ge thin films are rapidly melted into the deep region upon excimer-laser irradiation. In the partial melting regime (70–200 mJ/cm^2), the maximum temperature remains close to the melting temperature of a-Ge, because the excimer-laser fluence is consumed on the latent heat of phase transformation. In the complete melting regime (200–250 mJ/cm^2), molten Ge films are kept in the liquid state and the latent heat is not released when cooled below the melting temperature. The undercooled liquid Ge solidified rapidly and the latent heat is released simultaneously from the entire thickness. The longest melt duration of 90-nm-thick a-Ge thin films is approximately 200 ns. It is remarkable that the longest melt duration of Ge thin films is less than that of Si thin films of the same thickness because of low latent heat compared

with that of Si thin films [20].

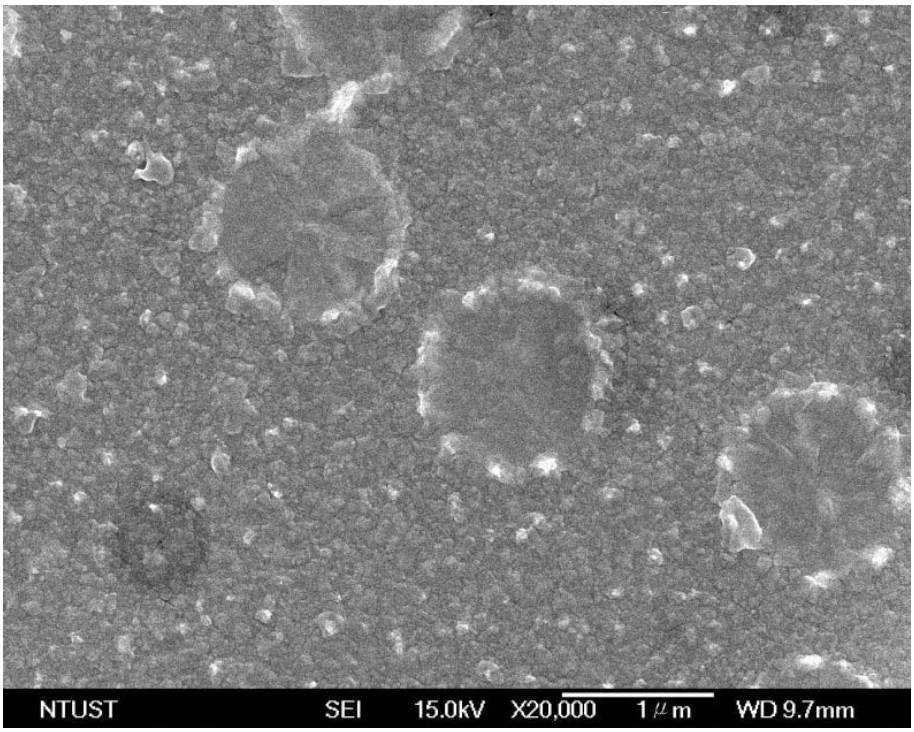

Fig. 10. FE-SEM micrograph of disc-shaped grain with a diameter of 0.8 μm in the complete melting regime.

Figure 10 shows a FE-SEM micrograph of disc-shaped grain with a diameter of approximately 0.8 μm in the complete melting regime. As can be seen, it is apparent that the defects in the disc-shaped grain are related to the low-angle grain boundaries. This disc-shaped grain is mainly caused by the explosive crystallization combined with liquid-phase growth [18]. The planar defects are found to be mainly twin boundary. This result is in good agreement with the observation of Ge thin films by Mulato et al. [21] and that of Si thin films in our previous work [9]. The micro-twinning mechanism of Si thin films has been reported by Liu et al. [22]. It is found by Morimoto et al. [23] that the solutions for minimizing the density of defects arise from the micro-twin growth mechanism.

4. Conclusions

Melting and recrystallization dynamics of Ge thin films during ELC are studied by TRORT measurements, FE-SEM, and micro-Raman spectroscopy. The disc-shaped grains with a diameter of approximately 0.8 μm in the complete melting regime with a melt-phase duration of approximately 141–200 ns are fabricated by a short-pulse XeF ELC. Ge thin films are rapidly melted and solidified due to low latent heat compared with Si thin films. Transmissivity in the TRORT measurements provides a prompt evaluation of excimer-laser fluence during mass production of high-performance TFTs. These results show the possibility of fabricating poly-Ge TFTs under appropriate conditions by ELC, which are essential for the device-to-device uniformity of high-performance TFTs. The twin defects are observed for poly-Ge

thin films after ELC. Eliminating the twin-defect density of poly-Ge thin films fabricated by short-pulse ELC is required in future studies. The grain size of poly-Ge, however, is not satisfactorily large for fabricating the single-grain Ge TFTs. Solutions to this issue by using a heat-retaining layer with a suitable absorption coefficient in the sample have been clarified and will be presented in a future paper.

Acknowledgments

The author would like to thank Professors W. C. Yeh and J. Y. Jeng of the National Taiwan University of Science and Technology for stimulating discussions and assistance with related experimental apparatus. The skillful technical assistance of Mr. C. P. Hsiao of the National Taiwan University of Science is highly appreciated.

References

1. H. Watakabe, T. Sameshima, H. Kanno, and M. Miyao, *Thin Solid Films*, **508**, 315 (2006).
2. S. Uchikoga and N. Ibaraki, *Thin Solid Films*, **383**, 19 (2001).
3. D. Shahrjerdi, B. Hekmatshoar, S. S. Mohajerzadeh, et al., *J. Electron. Mater.*, **33**, 353 (2004).
4. G. Masini, V. Cencelli, L. Colace, et al., *Appl. Phys. Lett.*, **80**, 3268 (2002).
5. R. L. Chapman, J. C. C. Fan, H. J. Zeiger, and R. P. Gale, *Appl.Phys. Lett.*, **37**, 292 (1980).
6. R. K. Sharma, S. K. Bansal, R. Nath, and G. P. Srivastava, *Thin Solid Films*, **97**, 1 (1982).
7. C. C. Kuo, *J. Russ. Laser Res.*, **28**, 383 (2007).
8. C. C. Kuo, W. C. Yeh, J. F. Lee, and J. Y. Jeng, *Thin Solid Films*, **515**, 8094 (2007).
9. C. C. Kuo, W. C. Yeh, C. P. Hsiao, and J. Y. Jeng, *J. Optoelectron. Adv. Mater.*, **54**, 484 (2007).
10. C. C. Kuo, W. C. Yeh, C. B. Chen, and J. Y. Jeng, *Thin Solid Films*, **515**, 1651 (2006).
11. B. Rezek, C. E. Nebel, and M. Stutzmann, *Jpn J. Appl. Phys.*, **38**, L1083 (1999).
12. J. Solis and C. N. Afonso, *J. Appl. Phys.*, **72**, 2125 (1992).
13. J. Boneberg and P. Leiderer, *Phys. Stat. Sol. (a)*, **166**, 643 (1998).
14. P. V. Santos, A. Trampert, F. Dondeo, et al., J. Appl. Phys., **90**, 2575 (2001).
15. S. A. Lyon, R. J. Nemanich, N. M. Johnson, and D. K. Biegelsen, *Appl. Phys. Lett.*, **40**, 316 (1982).
16. R. Messier, T. Takamori, and R. Roy, *Solid State Commun.*, **16**, 311 (1975).
17. G. E. Jellison and D.H. Lowndes, *Appl. Phys. Lett.*, **47**, 718 (1985).
18. M. O. Thompson, G. J. Galvin, J. W. Mayer, et al., *Phys. Rev. Lett.*, **52**, 2360 (1984).
19. D. Agassi, *J. Appl. Phys.*, **55**, 4376 (1984).
20. C. C. Kuo, W. C. Yeh, J. F. Lee, and J. Y. Jeng, in: *Abstracts of the International Manufacturing Leaders Forum [IMLF 2006]* (Taipei, Taiwan, October 23–25, 2006), p. 32 [http://www.itri.org.tw/eng/conference/conf-show-s.jsp].
21. M. Mulato, D. Toet, G. Aichmayr, et al., *Appl. Phys. Lett.*, **70**, 3570 (1997).
22. A. C. Y. Liu, J. C. McCallum, and W. L. Jung, *J. Mater. Res.*, **16**, 3229 (2001).
23. Y. Morimoto, S. Nakanishi, N. Oda, et al., *J. Electrochem. Soc.*, **141**, 1 (1994).